Metrol. Meas. Syst., Vol. XXI (2014), No. 4, pp. 675–684.

PAN POLSKA AKADEMIA NAUK

METROLOGY AND MEASUREMENT SYSTEMS

Index 330930, ISSN 0860-8229

www.metrology.pg.gda.pl

M&MS

BARRIER DETECTORS VERSUS HOMOJUNCTION PHOTODIODE

P. Martyniuk, W. Gawron

Institute of Applied Physics, Military University of Technology, 2 Kaliskiego Str., 00-908 Warsaw, Poland, (✉ *pmartyniuk@wat.edu.pl, +48 22 6839673*)

Abstract

In the last two decades several new concepts of photodetectors to improve their performance have been proposed. New strategies are especially addressed to the group of so called high-operating-temperature detectors where – apart from increasing of operating temperature – both the size and power consumption reduction is expected. In this paper a new strategy in the photo-detector design is presented - the barrier detectors: C_nBn; C_nBnN^+, C_pBn and unipolar barrier photodiodes. In spite of considering barrier detectors based on $A^{III}B^V$ bulk compounds and type-II superlattices as having theoretically a better performance than those based on HgCdTe, the latter compound is also used to fabricate barrier detectors. Among many new applications of barrier detectors the detection of explosives can be extremely important due to an increased threat of terrorist attacks. This paper presents the status of the barrier detectors and compares the performance of mid-wave HgCdTe barrier detectors and unipolar barrier photodiodes.

Keywords: BIRD, C_nBn, C_nBnN^+, C_pBn, C_pBnN^+, unipolar barrier photodiode.

© 2014 Polish Academy of Sciences. All rights reserved

1. Introduction

The standard defining the reduction of size, weight and power consumption of the infrared radiation (IR) detection system (SWaP - size, weight, and power conditions) is a source of the newest trends in IR detectors. Additionally, the requirement of uncooled operation becomes important owing to the fact that cooling of IR detection systems restricts the area of their applications [1]. In this context, developing new types of higher operation temperature (HOT) systems is significant, where the detectivity, the high frequency operation and the multispectral response enforce the development of new strategies. A proper control of the dark current components is a significant element allowing to increase the performance of IR detectors. Potential solutions could be found in the photon detector group. However, up till now the highest performance is reached at the temperatures below 200 K. Among the new technologies of HOT IR detectors the barrier infrared detectors (BIRD) - proposed by White for the very first time in 1983 [2] - should be listed. The barrier implementation allows filtering unwanted dark current components without impeding photo-generated carriers at the same time [3]. Surface currents, Shockley-Read-Hall (SRH) generation recombination (GR) currents from the depletion layer, tunneling (band-to-band [BTB] and trap-assisted tunneling [TAT]) currents have been eliminated with a great success by implementation of the barrier to the detector structure [4]. In addition, the barrier incorporation decreases a number of processing steps, making the technology of detectors more efficient. The barrier detectors are currently fabricated from bulk InAs, InAsSb and type-II superlattices (T2SLs); InAs/Ga(In)Sb being considered as a potential competitor of HgCdTe [5−10]. Many mid-wave (MWIR) structures with barriers were proposed and fabricated to include nBn, pBn, pBp-structures, “M”-, “W”-, “N”-layers (based on T2SLs). The complementary barrier infrared detector CBIRD and pBiBn allow to decrease the dark current and increase the quantum efficiency [11−17]. Among many new applications of HOT barrier detectors, the detection of explosives becomes extremely important due to an increased threat of terrorist attacks [18]. This paper presents the status of the barrier detectors

Article history: received on Sep. 01, 2014; accepted on Oct. 14, 2014; available online on Dec. 15, 2014; DOI: 10.2478/mms-2014-0058.

Brought to you by | Politechnika Swietokrzyska
Authenticated
Download Date | 1/27/15 2:11 PM

and compares the performance of MWIR HgCdTe barrier detectors and unipolar barrier photodiodes.

2. Barrier detectors

The very first paper related to unipolar barrier detectors was published by White, who proposed an architecture consisting of a narrow band-gap absorber and a wide gap thin barrier. Since Maimon and Wicks paper was published in 2006, the growing interest in barrier structures has been observed [19]. The concept of a unipolar barrier detector is based on lacking of the valence band offset (VBO) between the barrier and absorber layers allowing an unimpeded flow of minority carriers and blocking of majority carriers at the same time in structures C_nBn, where C_n is a cap/contact n-type layer (CL) made of either the same material as the absorber or a completely different material lattice matched to the barrier (B means an n-type wide gap barrier). Among the barrier structures the simplest - in terms of technology - is the nBn detector shown in Fig 1 (a). The essential condition to fabricate the nBn detector is a growth of the wafer with the same type of doping in constituent layers, especially in the barrier and the absorber, in order to restrict the SRH GR mechanism in the depletion region (between barrier and absorber layers) being decreased in comparison with a traditional p-n photodiode. The barrier should be a lattice matched to the absorber region and located close to the contact. This location of the barrier blocks the dark current associated with the majority carriers and the surface current, without impeding the photocurrent, what is shown in Fig 1 (b). The barrier does not block any dark current GR mechanism in the absorber region, while lack of a p-n junction allows to eliminate the influence of SRH GR (especially in $A^{III}B^{V}$).

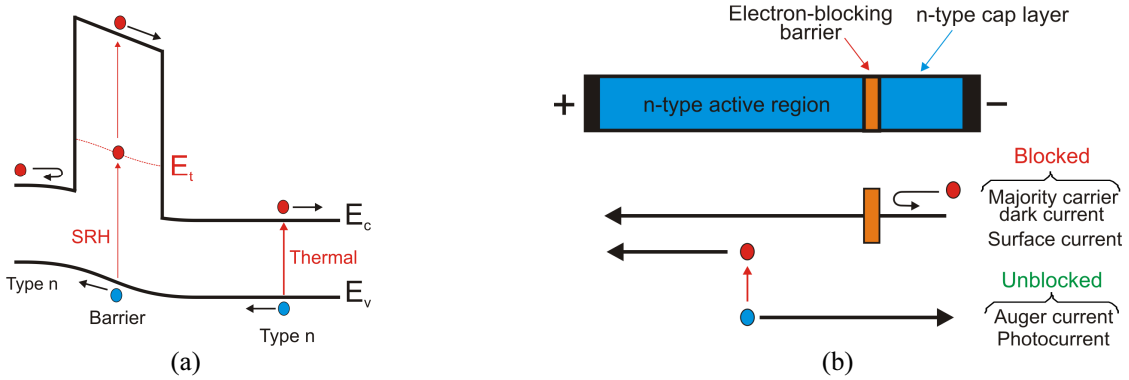

Fig. 1. A theoretical band-gap diagram of the nBn detector (a) and spatial makeups of the current component contribution in the barrier nBn structure (b).

The capability of a simple barrier detector is presented in Figure 2, where the Arrhenius [log (J_{DARK}) versus T^{-1}] plot of the dark current in a conventional p-n diode and the nBn structure is depicted. The diffusion current normally may be expressed by the relation ~ $T^3\exp(-E_{g0}/k_BT)$, where E_{g0} stands for the band gap extrapolated to the zero temperature T, k_B is the Boltzmann's constant. The GR current varies as ~ $T^{3/2}\exp(-E_{g0}/2k_BT)$ and is considered to be dominated by the generation of electrons and holes by SRH traps in the depletion region [20]. Assuming that the nBn detector is nearly lacking of the depletion region, the GR contribution to the net dark current from the absorber layer is limited. The solid red line (nBn) is an extension of the high temperature diffusion limited region to temperatures below T_C, which is defined as the crossover temperature at which the diffusion and GR currents are equal. In the low-temperature region the nBn detector should exhibit a higher signal-to-noise ratio in comparison with a conventional p-n diode operating at the same temperature, and operate at a higher temperature with the same J_{DARK}.

Brought to you by | Politechnika Swietokrzyska
Authenticated
Download Date | 1/27/15 2:11 PM

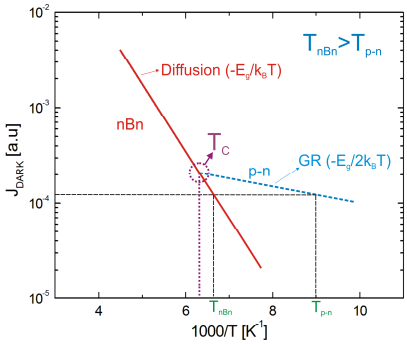

Fig. 2. The Arrhenius plot of the dark current in a standard p-n diode and nBn detector.

Apart from C_nB_nn structures, Klipstein and Klem proposed structures with the p-type (C_p) contact layer, where -similarly to C_n - C_p is fabricated from either the same material or different but opposite doping than the absorber layer [20, 21]. Incorporation of the p-type contact layer in a C_pBn architecture allows to lower the turn on voltage (bias to where VBO does not influence the minority carrier transport) in comparison with C_nBn structures.

Fig. 3. Schematic band profile configurations for n-type base (a) and p-type base (b) barrier detectors.

Lack of the depletion layer in the barrier-absorber heterojunction creates an opportunity for materials where SRH GR mechanisms efficiently contribute to the net dark current (including mainly $A^{III}B^{V}$ materials, where T_{SRH} is reported up to 700 ns at the best). MWIR barrier structures are successfully fabricated with $A^{III}B^{V}$ compounds including: InAs/B-AlAsSb, InAsSb/B-AlAsSb T2SLs InAs/GaSb/B-AlGaSb/T2SLs [22]. Introduction of 6.1 Å $A^{III}B^{V}$ T2SLs allowed to grow and fabricate an ideal barrier detector, where - thanks to energy band gap engineering (ability to tune the positions of the conduction and valence bands independently) - VBO was nearly leveled. The condition of VBO = 0 eV is not the only requirement which must be met during the detector developing procedure. The barrier structure should be characterized by a large conduction band offset (CBO). T2SLs InAs/GaSb are predicted to be the only material system to compete with HgCdTe, therefore this material plays an important role as a potential material for IR detectors fabrication. Except bulk AlGaSb, barriers could be effectively grown from T2SLs InAs/GaSb depending on both InAs and GaSb layer thickness. In case of T2SLs, a mutual lineup of the energy bands of the constituent layers exhibits unique properties. The top of the GaSb valence band is located above the bottom of the InAs conduction band which locates electrons in InAs and holes in GaSb layers, respectively. Such a spatial separation of electrons and holes theoretically suppresses the Auger GR process. The effective energy band-gap, similarly to HgCdTe, can be tailored within a wide range of energy up to 300 meV. The electron effective mass in InAs/GaSb T2SLs does not depend strongly on the energy band-gap value, whereas this dependence is stronger for HgCdTe, reducing contribution of the tunneling currents in the T2SLs structures [23]. At the current status of the T2SLs InAs/GaSb technology, the recombination by deep SRH centers is found to be dominant, as long as the carrier lifetime is taken into consideration (for $T > 150$ K carrier lifetimes are even lower than 20 ns [24]).

It must be stressed, that the 6.1 Å $A^{III}B^{V}$ compound family - InAs/Ga(In)Sb/AlSb - allows for many modifications of the detector structure. Aifer *et al.* proposed a "W"-structure InAs/GaInSb/InAs/AlGaInSb shown in Fig 4 (a), which could be used as either a barrier for

Brought to you by | Politechnika Swietokrzyska
Authenticated
Download Date | 1/27/15 2:11 PM

electrons and holes or an absorber layer, thanks to the wavefunction overlapping [12]. Nguyen *et al.* proposed an "M"-structure GaSb/InAs/GaSb/AlSb presented in Fig. 4 (b) and mainly used as barrier layers [13−15]. Active layers could be grown with "N" structures proposed by Salihoglu *et al.,* presented in Fig. 4 (c) [16]. Klem *et al.* proposed an InAsPSb/B-AlAsSb architecture (long minority carrier lifetimes in comparison to the T2SLs InAs/GaSb being limited by short SRH lifetimes) for the applications where cut-off wavelengths shorter than 4.2 μm are needed [25].

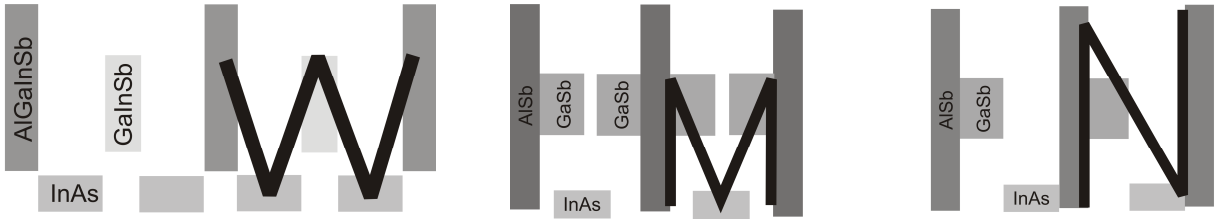

Fig. 4. Energy band diagrams of "W" (a), "M" (b) and "N" (c) structures.

The growth of a barrier structure exhibiting VBO = 0 eV between the barrier and the absorber for HgCdTe (MWIR HgCdTe exhibits 100−400 meV VBO depending on both absorber/barrier composition and doping) has turned out to be difficult in terms of technology, yet the research on this structures has been developing owing to problems with p-type doping in the MBE technology.The HgCdTe nBn devices operating in MWIR range were presented by Itsuno *et al.* [26]. The HgCdTe ternary alloy is a close to ideal infrared material system. Its position is conditioned by three key features: the composition-dependent tailorable energy band gap, the large optical coefficients that enable a high quantum efficiency, and the favorable inherent recombination mechanisms leading to a long carrier lifetime and a high operating temperature. In addition, an extremely small change of the lattice constant with the composition makes it possible to grow high quality layered heterostructures. However, the existence of VBO in HgCdTe-based nBn detectors creates several issues limiting their performance. Depending on the wavelength of operation, a relatively high bias, typically greater than the bandgap energy, is required to be applied to the device in order to collect all of the photogenerated carriers. This leads to a strong BTB and TAT tunneling due to a high electric field within the depletion layer. Parameters of the MCT devices are still better than those employing other materials, including $A^{III}B^{V}$ based T2SLs InAs/GaSb. In spite of many advantages, HgCdTe is technologically extremely difficult to grow. Hg bonding reduces the strength of a material, resulting in weak mechanical properties and creating difficulties in a material processing. Moreover, a high Hg vapor pressure makes the composition control over a large area difficult. This justifies an effort to find materials alternative to HgCdTe among compounds from the $A^{III}B^{V}$ family with a larger covalent bonding participation, which in turn results in a better stability of these compounds in comparison to compounds from the $A^{II}B^{VI}$ group.

A further strategy in development of HgCdTe nBn detectors should be focused on decreasing or even removing the VBO in the barrier layer, which will result in a lower operating bias, a lower dark current, and an ability to operate at higher temperatures. Schubert *et al.* proposed an approach to circumvent VBO by appropriate doping the interface regions [27].

Unipolar barriers can be efficently implemented into conventional p-n photodiodes [28, 29]. Two possible locations arbitrated on blocking the dark current components can be listed. The locations are shown in Fig. 5: in the p-type layer (out of the depletion layer) (a) and in the n-type layer (in the edge of the depletion layer) (b). In the first case, the surface contribution to the net dark current is blocked, while the diffusion, GR and TAT, and BTB are not restricted. In the second case, the dark current generated in the junction area is effectively blocked, what is shown in Fig. 5 (a) and (b), respectively.

Brought to you by | Politechnika Swietokrzyska
Authenticated
Download Date | 1/27/15 2:11 PM

Fig. 5. Theoretical band diagrams of p-n photodiodes with barriers in the p-type (a) and the n-type (b) region.

3. Simulation procedure and results

Table 1 shows parameters taken in modeling of MWIR HgCdTe barrier detectors. The doping profiles were simulated by applying the Gaussian tail model. The active layer composition was assumed to be in the MWIR range, x = 0.3, according to the nBn HgCdTe structure presented by Itsuno *et al.* [26].

Table 1. Parameters assumed in modeling of MWIR barrier detectors.

$C_{n(p)}Bn(N^+)$	**n**	**P**	**B**	**n**	**N^+**	
N_A, N_D [cm^{-3}]	7×10^{14}, 10^{16}	7×10^{14}, 10^{16}	2×10^{15}	10^{14}	10^{16}	
Composition, x	0.33	0.33	0.3→0.64→0.3	0.3	0.3→0.64	
Geometry, d [μm]	0.16	0.16	0.14	2.74	0.2	
Barrier diodes	**p**	**B**	**p**	**n**	**B**	**n**
N_A, N_D [cm^{-3}]	7×10^{14}	2×10^{15}	7×10^{14}	7×10^{14}	2×10^{15}	7×10^{14}
Gauss tail, dx [μm]	0.02	0.02	0.02	0.02	0.02	0.02
Composition, x	0.3	0.3→0.35→0.6 →0.35→0.3	0.3	0.3	0.3→0.35→0.6 →0.35→0.3	0.3
Geometry, d [μm]	1	0.14	1	1	0.14	1
Electrical area, A [μm^2]	120×120					
Overlap matrix, F_1F_2	0.15					
Trap energy level, E^{Trap} [eV]	$E_g/2$					
Trap concentration, N_{Trap} [cm^{-3}]	10^{13}					
Carrier capture cross sections, σ_n, σ_p [cm^2]	1.6×10^{-16}; 8.5×10^{-15}					

Theoretical modeling of the MWIR HgCdTe barrier detectors has been performed by numerical solving of the Poisson's equation and the carrier current continuity equations by a commercially available APSYS platform (Crosslight Inc.) with the Newton-Richardson method of nonlinear iterations implemented [30]. The applied model incorporates both electrical and optical properties, including an influence of the radiative (RAD), Auger (AUG), SRH GR, at any location within the device, and BTB as well as TAT tunneling mechanisms at the barrier-absorber heterojunction. We incorporated AUG recombination mechanisms using the theory developed by Casselman *et al.* [31]. The APSYS numerical platform requires the HgCdTe composition, temperature and doping dependence on the electron affinity, bandgap, intrinsic concentration, mobility and effective masses. The bandgap was obtained from the paper of Hansen *et al.* [32]. The low-field electron mobility was taken after Scott's study, where the hole mobility was basically taken as 0.01 of the electron mobility [33]. The intrinsic concentration, composition and temperature dependence was calculated based on the Hansen *et al.* model [34]. Ohmic contacts are modeled as Dirichlet boundary conditions - electron and hole quasi-Fermi levels are equal and assumed to be at the voltage of the biased electrode, i.e., $E_{fn} = E_{fp} = V$. For the TAT simulation the Hurkx *et al.* model was implemented [35].

Brought to you by | Politechnika Swietokrzyska
Authenticated
Download Date | 1/27/15 2:11 PM

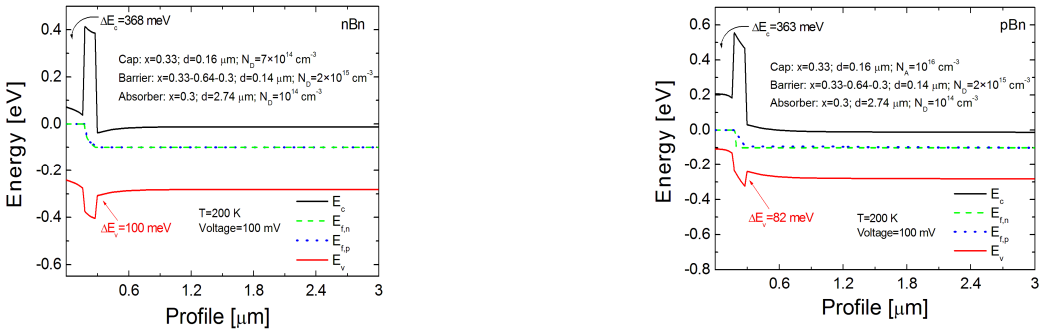

(a) (b)

Fig. 6. Energy band diagrams for nBn (a) and pBn (b) HgCdTe barrier detectors.

The calculated energy band diagrams for the nBn and pBn detector structures for a low bias, V = 100 mV, are depicted in Fig. 6 (a) and (b), respectively. Unlike the pBn architecture, the nBn type detector should be reversely biased (i.e. a positive voltage should be applied to the absorber contact). A proper type of doping the thin CL doping influences the ΔE_v allowing a nearly unimpeded flow of holes to the contact, permitting zero bias operation. The barrier heights, ΔE_c, are comparable for both structures having different levels of CL doping: $N_D = 7\times10^{14}$ cm^{-3} and $N_A = 10^{16}$ cm^{-3} , respectively. At the same time the barrier in the valence band, ΔE_v , is slightly higher for the nBn (ΔE_v = 100 meV) in comparison with the p-type CL (ΔE_v = 82 meV) which should be evident in the dark current (J_{DARK}) versus voltage characteristics.

Similar considerations were performed for nBnN$^+$ and pBnN$^+$ structures and energy band diagrams of the detectors at a low bias, V = 100 mV, and are depicted in Fig. 7 (a) and (b), respectively. Similarly, the pBnN$^+$ architecture enables near zero operation, where ΔE_{v1} should be < 55 meV (ΔEv_1 and $\Delta E_v < 3k_BT$) for T = 200 K. An extra N$^+$ contact layer in the nBnN$^+$ and the pBnN$^+$ slightly influences both ΔE_{c1} (368→373 meV; 363→370 meV) and ΔE_{v1} (100→92 meV; 82→78 meV) in comparison with the nBn and pBn architectures.

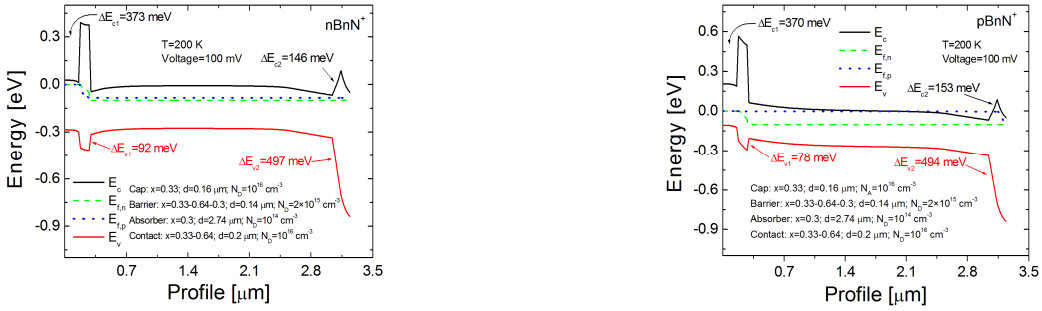

(a) (b)

Fig. 7. Energy band diagrams for nBnN$^+$ (a) and pBnN$^+$ (b) HgCdTe barrier detectors.

The barrier influence is clearly evident in Fig. 8 (a) and (b), respectively, where the J_{DARK} versus voltage characteristics and the temperature are shown for nBn, pBn, nBnN$^+$ and pBnN$^+$. The turn on voltage is assumed to be V = 350 mV for nBn and 200 meV for pBn structures, respectively. In the case of the nBn and pBn structures the simulations were performed for the following contact layer doping: $N_D = 7\times10^{14}$ cm^{-3} and $N_D = N_A = 10^{16}$ cm^{-3}. An extra N$^+$ ($N_D = 10^{16}$ cm^{-3}) contact layer reduces the turn on voltage to 200 mV for the nBnN$^+$ and to 50 mV for the pBnN$^+$ detector, respectively. In the considered temperature T = 200 K and the turn on voltage level, J_{DARK} is extremely sensitive to bias, while above the turn on voltage J_{DARK} is less voltage-dependent and the dark current saturation is observed. ΔE_v for V = 350 mV (nBn) is comparable with 55 meV ($3k_BT$), which means that holes are nearly freely transported to the CL giving contribution to the net J_{DARK}. In the simulated voltage range no tunneling contribution occurs, which is mainly caused by the fact that the barrier structure is diffusion and GR limited.

Brought to you by | Politechnika Swietokrzyska
Authenticated
Download Date | 1/27/15 2:11 PM

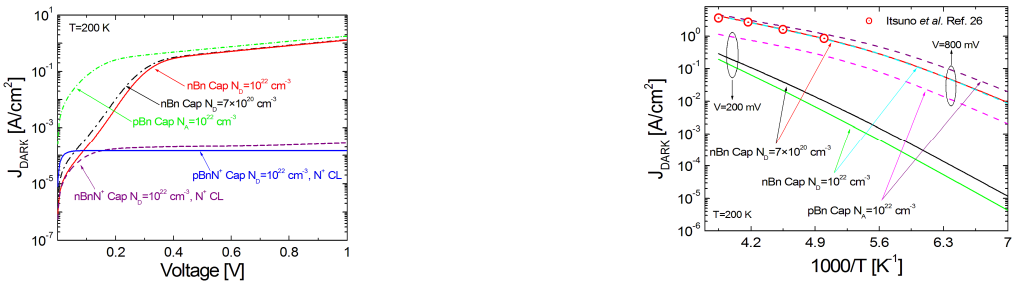

Fig. 8. J_{DARK} versus voltage, T = 200 K (a) and versus the reciprocal temperature, V = 200 and 800 mV (b) for the considered barrier detectors.

The J_{DARK} characteristics at each simulated temperature exhibits a current plateau above the turn on voltage level for structures with an extra N^+ barrier. This extra N^+ layer, creating mainly an extra barrier in the valence band (ΔE_{v2}), effectively limits the hole injection to the absorber layer. It must be stressed that J_{DARK} slightly increases with the applied voltage due to the fact that in nBn and pBn structures the hole injection is not restricted. It is clearly seen, that introducing the p-type CL to the barrier structure reduces the barrier in the valence band (ΔE_{v1}) allowing an unimpeded transport of holes to the cap layer. Comparing the nBn and pBn structures for the same level but opposite doping $N_D = N_A = 10^{16}$ cm^{-3}, J_{DARK} for the nBn structure is lower in comparison with the pBn structure. This behaviour should be attributed to ΔE_c and ΔE_v dependence on bias (for V = 200 mV, ΔE_v = 100→82 meV and ΔE_c = 368→363 meV [see Fig. 6 (a) and (b)].

Figure 8 (b) presents the dark current characteristics versus the inverse temperature for the considered nBn and pBn structures, simulated for two selected voltages: V = 200 and 800 mV. The J_{DARK} temperature dependence for both analyzed CL doping: $N_D = 7\times10^{14}$ and 10^{16} cm^{-3} , is related to the ΔE_c and ΔE_v dependence on T (for nBn: ΔE_c = 373→387 meV, ΔE_v = 100 meV; for pBn ΔE_c = 368→380 meV, ΔE_v = 82→94 meV for T = 200→160 K). Increasing the CL doping, $N_D = 7\times10^{14}\rightarrow10^{16}$ cm^{-3}, J_{DARK} slightly decreases for the nBn structure. The simulation results are compared to the measured ones given by Itsuno *et al.* (V = 800 mV, n-type CL doping $N_D = 7\times10^{14}$ cm^{-3}) [26]. The proper agreement between simulation and experimental results was reached.

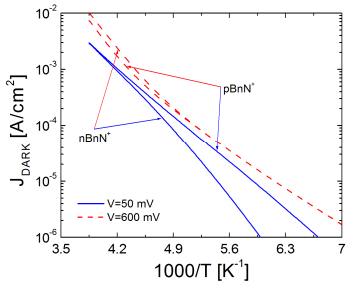

Fig. 9. J_{DARK} versus the reciprocal temperature, V = 50 and 600 mV for the $nBnN^+$ and $pBnN^+$ barrier detectors.

Similar considerations for the $nBnN^+$ and $pBnN^+$ structures were presented in Fig. 9. A charcteristic two slope behaviour is observed above the turn on voltage level for both analyzed $nBnN^+$ and $pBnN^+$ structures. The estimated T_C for the p-type CL is 205 K, while for the n-type CL is 211 K. Above these temperatures the diffusion contribution plays a dominant role. It is believed, that ΔE_{v1} ($nBnN^+$ - 92 meV; $pBnN^+$ - 78 meV) plays a dominant role and explains that difference. The experimental data for the diffusion contribution were fitted by $\sim T^3 \exp(-q0.269/k_BT)$, while the GR component could be fit by the relation: $\sim T^{1.5} \exp(-q0.269/2k_BT)$ for the $pBnN^+$ structure, where 0.269 eV corresponds to E_g at T = 200 K for x = 0.3.

Simulated energy band diagrams for p-n diodes with an extra barrier in the p-type region (a) and the n-type region (b) are presented in Fig. 10. The p-n junction doping and both n-type and p-type contact layers were assumed to be $N_D = N_A = 7\times10^{14}$ cm^{-3}, while the barrier doping in the p-type region was assumed to be p-type doped, $N_A = 10^{15}$ cm^{-3} and in the n-type region

Brought to you by | Politechnika Swietokrzyska
Authenticated
Download Date | 1/27/15 2:11 PM

$N_D = 10^{15}$ cm^{-3}, respectively (the barrier composition $x = 0.64$). The simulations were performed for $T = 200$ K and $V = 200$ mV. A barrier in the valence band, ΔE_v, for both structures was estimated to be in the same range, 83−84 meV, while in the conduction band, ΔE_c, is by 26 meV higher for a barrier in the p-type region.

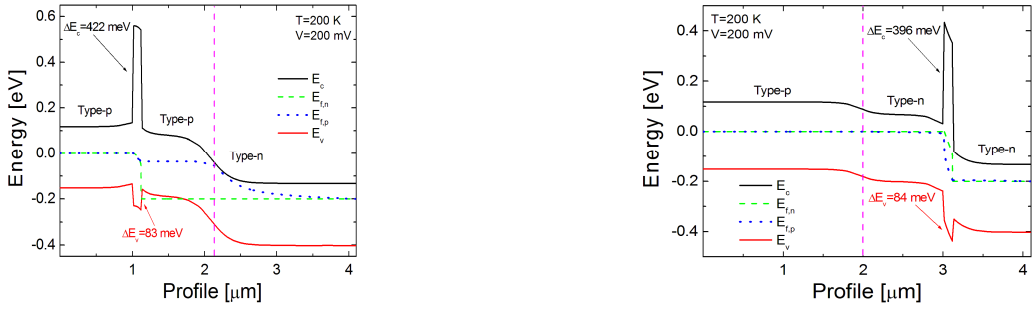

Fig. 10. Energy band diagrams for p-n diodes with an extra barrier in the p-type (a) and the n-type region based on HgCdTe (b) for $T = 200$ K and $V = 200$ mV.

The barrier implementation to a p-n diode lowers J_{DARK} by nearly two orders of magnitude in comparison with the structure with a barrier in the p-type region in the analyzed voltage region. The structure in the n-type region enables to reach even four orders of magnitude lower J_{DARK} in comparison with a standard p-n diode and two orders of magnitude than the structure with a barrier in the p-type region for $V < 200$ mV. An applied bias lowers ΔE_c (396→374 meV) and - much more effectively - ΔE_v (84→62 meV) in the structure with a barrier in the n-type region contributing to increase of J_{DARK} for a higher voltage. ΔE_c and ΔE_v keep a constant value versus voltage for the structure with a barrier in the p-type.

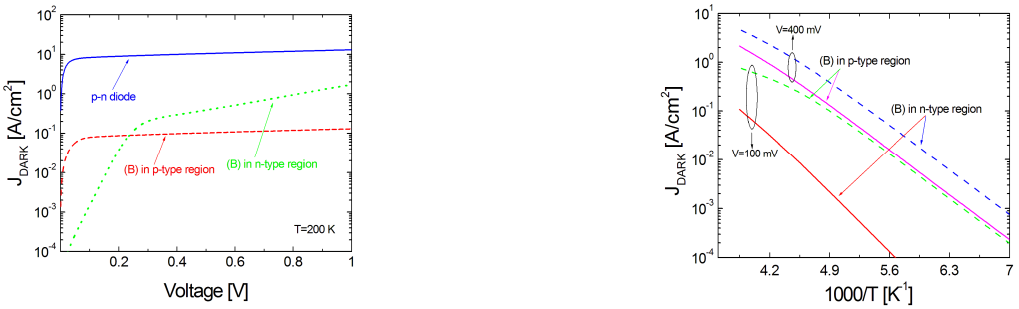

Fig. 11. J_{DARK} versus voltage, $T = 200$ K (a) and the reciprocal temperature, $V = 100$ and 400 mV (b) for p-n diodes with barriers in the p-type and n-type regions.

An influence of the barrier composition on J_{DARK} for p-n diodes with extra barriers in both n- and p-type regions is presented in Fig. 12 for $V = 100$ and 400 mV. For p-n diodes with a barrier in the p-type region J_{DARK} saturates for the barrier composition, $x > 0.42$ for both analyzed voltages. For the second analyzed structure with a barrier in the n-type region, J_{DARK} keeps a constant value for $x > 0.56$ ($V = 400$ mV), while for $V = 100$ mV the dark current decreases with a higher composition.

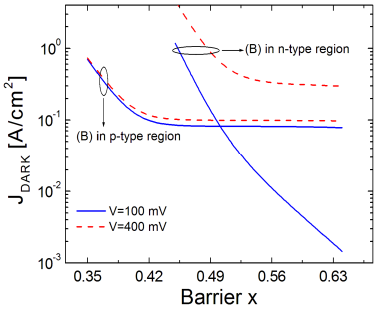

Fig. 12. J_{DARK} versus the barrier composition (barrier doping, $N_D = N_A = 10^{15}$ cm^{-3}) for p-n diodes with barriers in the p-type and n-type regions.

Brought to you by | Politechnika Swietokrzyska
Authenticated
Download Date | 1/27/15 2:11 PM

4. Conclusions

Up to now, at this stage of the IR detector development, the HgCdTe privileged position is unquestionable. New types of IR detectors are implemented into HgCdTe technology including barrier structures and unipolar p-n photodiodes. Thanks to barriers, the dark current could be effectively reduced in presented structures. A further work requires an improvement in the HgCdTe technology in terms of limiting VBO in order to allow an unimpeded transport of photogenerated carriers.

Acknowledgements

This paper has been done under the financial support of the Polish National Science Centre, Project: **UMO-2012/07/D/ST7/02564** and **PBS 849**. The authors thank Professor Antoni Rogalski for a helpful and beneficial discussion.

References

[1] Rogalski, A. (2011). *Infrared Detectors,* second edition. CRC Press, Boca Raton.

[2] White, A. (1983). Infrared detectors. *U.S. Patent* 4.679.063.

[3] Klipstein, P. (2003). Depletionless photodiode with suppressed dark current and method for producing the same. *U.S. Patent* 7.795.640.

[4] Klipstein, P. (2008). XBn barrier photodetectors for high sensitivity operating temperature infrared sensors. In *Proceedings of SPIE* 2008. Orlando, USA, 69402U-1–11.

[5] Brown, G. J. (2005). Type-II InAs/GaInSb superlattices for infrared detection: an overview. In *Proceedings of SPIE* 2005. Orlando, USA, 5783, 65–77.

[6] Ting, D. Z., Soibel, A., Höglund, L., Nguyen, J., Hill, C. J., Khoshakhlagh, A., Gunapala, S. D. (2011). Type-II superlattice infrared detectors. In *Semiconductors and Semimetals*, edited by S.D. Gunapala, D.R. Rhiger, and C. Jagadish, Elsevier, Amsterdam.

[7] Itsuno, A. M., Philips, J. D., Velicu, S. (2011). Design and modeling of HgCdTe nBn detectors. *J. Elect. Mater*. 40(8), 1624–1629.

[8] D'Souza, A. I., Robinson, E., Ionescu, A. C., Okerlund, D., De Lyon, T. J., Rajavel, R. D., Sharifi, H., Yap, D., Dhar, N., Wijewarnasuriya, P. S., Grein, C. (2012). MWIR $InAs_{1-x}Sb_x$ nCBn detectors data and analysis. In *Proceedings of SPIE* 2012. Baltimore, USA, 835333-1–8.

[9] D'Souza, A. I., Robinson, E., Ionescu, A. C., Okerlund, D., De Lyon, T. J., Rajavel, R. D., Sharifi, H., Dhar, N. K., Wijewarnasuriya, P. S., Grein, C. (2013). MWIR InAsSb barrier detector data and analysis. In *Proceedings of SPIE* 2013. Baltimore, USA, 87041U-1–7.

[10] Velicu, S., Zhao, J., Morley, M., Itsuno, A. M., Philips, J. D. (2012). Theoretical investigation of MWIR HgCdTe nBn detectors. In *Proceedings of SPIE* 2012. San Francisco, USA, 82682X-1–13.

[11] Rodriguez, J. B., Plis, E., Bishop, G., Sharma, Y. D., Kim, H., Dawson, L. R., Krishna, S. (2007). nBn structure based on InAs/GaSb type-II strained layer superlattices. *Appl. Phys. Lett.* 91, 043514-1–2.

[12] Aifer, E. H., Tischler, J. G., Warner, J. H., Vurgaftman, I., Bewley, W. W., Meyer, J. R., Kim, J. C., Whitman, L. J. (2006). W-structured type-II superlattice long-wave infrared photodiodes with high quantum efficiency. *Appl. Phys. Lett*. 89(5), 053519-1–3.

[13] Nguyen, B. M., Razeghi, M., Nathan, V., Brown, G. J. (2007). Type-II "M" structure photodiodes: an alternative material design for mid-wave to long wavelength infrared regimes. In *Proceedings SPIE* 2007. USA, 64790S-1–10.

[14] Nguyen, B. M., Hoffman, D., Delaunay, P. Y., Razeghi, M. (2007). Dark current suppression in type II InAs/GaSb superlattice long wavelength infrared photodiodes with M-structure. *Appl. Phys. Lett*. 91(16), 163511-1–3.

Brought to you by | Politechnika Swietokrzyska
Authenticated
Download Date | 1/27/15 2:11 PM

[15] Nguyen, B. M., Hoffman, D., Delaunay, P. Y., Huang, E. K., Razeghi, M., Pellegrino, J. (2008). Band edge tunability of *M*-structure for heterojunction design in Sb based type II superlattice photodiodes. *Appl. Phys. Lett.* 93(16), 163502-1–3.

[16] Salihoglu, O., Muti, A., Kutluer, K., Tansel, T., Turan, R., Ergun, Y., Aydinli, A. (2012). "N" structure for type-II superlattice photodetectors. *Appl. Phys. Lett*. 101, 073505-1–4.

[17] Gautam, N., Myers, S., Barve, A. V., Klein, B., Smith, E. P., Rhiger, D., Plis, E., Kutty, M. N., Henry, N., Schuler-Sandyy, T., Krishna, S. (2013). Band engineering HOT midwave infrared detectors based on type-II InAs/GaSb strained layer superlattices. *Infrared Physics & Techol.* 59, 72−77.

[18] Wojtas, J., Rutecka, B., Popiel, S., Nawała, J., Wesołowski, M., Mikołajczyk, J., Cudziło, S., Bielecki, Z. (2014). Explosives vapors-concentrating and optoelectronic detection. *Metrology and Measurement Systems*, 21(2), 177–190.

[19] Maimon, S., Wicks, G. (2006). nBn detector, an infrared detector with reduced dark current and higher operating temperature. *Appl. Phys. Lett.* 89, 151109-1–3.

[20] Klipstein, P., Klin, O., Grossman, S., Snapi, N., Lukomsky, I., Aronov, D., Yassen, M., Glozman, A., Fishman, T., Berkowicz, E., Magen, O., Shtrichman, I., Weiss, E. (2011). XB*n* barrier photodetectors based on InAsSb with high operating temperatures. *Opt. Eng.* 50(6), 061002-1–10.

[21] Klem, J. F., Kim, J. K., Cich, M. J., Hawkins, S. D., Fortune, T. R., Rienstra, J. L. (2010). Comparison of nBn and nBp mid-wave barrier infrared photodetectors. In *Proceedings of SPIE 2010.* San Francisco, USA, 76081P.

[22] Ting, D. Z., Hill, C. J., Soibel, A., Nguyen, J., Keo, S. A., Lee, M. C., Mumolo, J. M., Liu, J. K., Gunapala, S.D. (2010). Antimonide-based barrier infrared detectors. In *Proceedings of SPIE 2010*. Orlando, USA, 76601R-1–12.

[23] Plis, E. A. (2014). InAs/GaSb type-II superlattice detectors. *Advances in Electronics* 246769-1–12.

[24] Wróbel, J., Martyniuk, P., Plis, E., Madejczyk, P., Gawron, W., Krishna, S., Rogalski, A. (2012). Dark current modeling of MWIR type-II superlattice detectors. In *Proceedings of SPIE* 2012. Baltimore, USA, 8353-1−16.

[25] Klem, J. F., Hawkins, S. D., Kim, J. K., Leonhardt, D., Shaner, E. A. (2013). GaSb-based infrared detectors utilizing InAsPSb absorbers. *J. Vac. Sci. Technol.* B 31(3), 03C115-1−7.

[26] Itsuno, A. M., Philips, J. D., Velicu, S. (2012). Mid-wave infrared HgCdTe nBn photodetector. *Appl. Phys. Lett.* 100(16), 161102-1−3.

[27] Schubert, E. F., Tu, L.W., Zydzik, G. J., Kopf, R. F., Benvenuti, A., Pinto, M. R. (1991). Elimination of heterojunction band discontinuities by modulation doping. *Appl. Phys. Lett.* 60(4), 466−468.

[28] Savich, G. R., Pedrazzani, J. R., Sidor, D. E., Maimon, S., Wicks, G. W. (2011). Dark current filtering in unipolar barrier infrared detectors. *Appl. Phys. Lett*. 99, 121112-1−3.

[29] Savich, G. R., Pedrazzani, J. R., Sidor, D. E., Maimon, S., Wicks, G. W. (2012). Use of unipolar barriers to block dark currents in infrared detectors. In *Proceedings of SPIE* 2012. Orlando, USA, 8022T.

[30] APSYS Macro/User's Manual ver. 2011. Crosslight Software, Inc. (2011).

[31] Casselman, T. N., Petersen, P. E. (1980). A comparison of the dominant Auger transitions in *p*-type (HgCd)Te. *Solid State Commun.* 33, 615–619.

[32] Hansen, G. L., Schmidt, J. L., Casselman, T. N. (1982). Energy gap versus alloy composition and temperature in $Hg_{1-x}Cd_xTe$. *J. Appl. Phys.*, 53(10), 7099−7101.

[33] Scott, W. (1972). Electron mobility in $Hg_{1-x}Cd_xTe$. *J. Appl. Phys.* 43(3), 1055−1062.

[34] Hansen, G. L., Schmidt, J. L. (1983). Calculation of intrinsic carrier concentration in $Hg_{1-x}Cd_xTe$. *J. Appl. Phys.*, 54(3), 1639−1640.

[35] Hurkx, G. A., Klaassen, D. B. M., Knuvers, M. P. G. (1992). A new recombination model for device simulation including tunneling. *IEEE Trans. Electron Devices*, 39(2), 331−338.

Brought to you by | Politechnika Swietokrzyska
Authenticated
Download Date | 1/27/15 2:11 PM